

Three-dimensional Imaging Method Incorporating Range Points Migration and Doppler Velocity Estimation for UWB Millimeter-wave Radar

Yuta Sasaki, *Non-member*, Fang Shang, *Member, IEEE*, Shouhei Kidera, *Member, IEEE*, Tetsuo Kirimoto, *Senior Member, IEEE* Kenshi Saho *Member, IEEE* and Toru Sato, *Member, IEEE*

Abstract—High-resolution, short-range sensors that can be applied in optically challenging environments (e.g., in the presence of clouds, fog, and/or dark smog) are in high demand. Ultra-wideband millimeter-wave radars are one of the most promising devices for the above applications. For target recognition using sensors, it is necessary to convert observational data into full 3-dimensional (3-D) images with both time-efficiency and high accuracy. For such conversion algorithm, we have already proposed the range points migration (RPM) method. However, in the existence of multiple separated objects, this method suffers from inaccuracy and high computational cost due to dealing with many observed range points. To address this issue, this study introduces Doppler-based range points clustering into the RPM method. The results from numerical simulations, assuming 140-GHz band millimeter radars, show that the addition of Doppler velocity into the RPM method results in more accurate 3-D images with reducing computational costs.

Index Terms—Range points migration(RPM), Multi-static UWB Doppler Radar, Short range sensing

I. INTRODUCTION

Short-range, millimeter-wave radar systems have significant advantages including higher spatial resolution and applicability to optically harsh environments (e.g., dark smog, fog, or strong back light) and show promise for various sensing applications such as collision-avoidance sensors for automobiles and watch sensors for elderly or disabled persons living alone. Recently, 140-GHz radar systems have attracted attention because this frequency minimizes the absorption of moisture vapor, allowing the detection of targets from automobiles in high-moisture environments. Moreover, the size of the transmitting and receiving modules can be considerably reduced, making the actual implementation of the system more flexible. Various studies on 3-D imaging algorithms focused on short-range sensing have been reported, most of which are based on the delay-and-sum (DAS) approach, for example, beamforming, time-reversal algorithms [1], and range migration methods [2] or Kirchhoff migration [3]. However, these studies required high computational costs to obtain full three-dimensional (3-D) voxel images and also suffered from limited accuracy for objects with continuous boundaries because of the pointwise target assumption.

To address these issues, a non-parametric, fast, 3-D imaging method called shape estimation algorithm based on boundary scattering transform and extraction of directly scattered waves (SEABED) was developed based on reversible transforms between the time delay and the target boundary [4]. However, this method has fundamental drawbacks; for example, it requires a range point connection procedure during pre-processing, which is difficult in richly interfered situations. The range points migration (RPM) method was developed as a promising method for solving this problem [5]. This method achieves a batch conversion from range points abbreviated as RP (a set of antenna location and observed range points) to scattering center points with one-to-one correspondence. The RPM method converts each range point (referred to as Main RP) to each scattering center by assessing the focusing degree using all surrounding RPs (called Sub RPs). Notably, this method resolves an inherent paring problem between the range and direction of arrival using a Gaussian kernel-based statistical approach. Thus, RPM is free from complicated pre-processing involving connecting or paring range points. This feature confers the significant advantages of both lower computational cost and higher accuracy for locating scattering centers on continuous boundaries, even in richly interfered cases.

Based on the above merits, the RPM method has been successfully applied to short range sensing issues, including the experimental validation [6], the through-the-wall extension [7] or the three-dimensional ultrasonography imaging issues [8]. In addition, the millimeter radar application assuming 140-GHz band UWB signal has been investigated using a multi-static configuration [9]. The multi-static configuration considerably reduces the time required for data acquisition compared to the radar scanning model, which is necessary for achieving real-time imaging. However, when a sensor receives many reflection echoes, assuming multiple objects or objects with complicated shapes, this method suffers from large computational cost and inaccuracy. This occurs because RPM assesses a focusing degree using all surrounding RPs (called SubRPs) during the conversion from targeted RPs (called Main RPs) to scattering points, and SubRPs might include unnecessary one. To improve the efficiency and accuracy of the RPM method, this paper introduces a Doppler velocity-based RP clustering algorithm that enhances imaging accuracy by selecting an appropriate set of SubRPs. While Doppler based data clustering or separation has been demonstrated in

Y. Sasaki, F. Shang, S. Kidera and T. Kirimoto are with the Graduate School of Informatics and Engineering, The University of Electro-Communications, Japan. E-mail: kidera@ee.uec.ac.jp K. Saho is with the College of Science and Engineering, Ritsumeikan University, Japan, T. Sato is with the Graduate School of Informatics, Kyoto University, Japan.

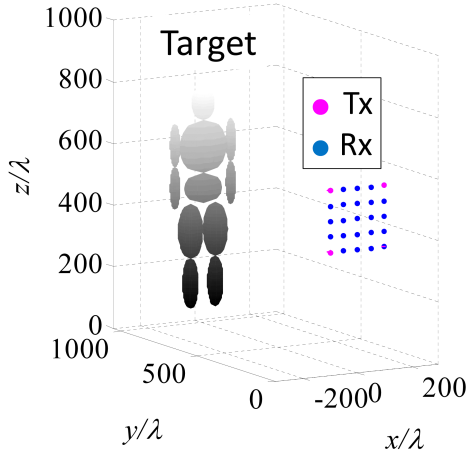


Fig. 1. System model.

lots of literature, there are no investigations for incorporating the RPM for improving both computational efficiency and accuracy. Furthermore, the proposed method can associate a Doppler velocity with each scattering center, which greatly assists in human body recognition as demonstrated in [10]. The results obtained from numerical simulations assuming 140 GHz band UWB radar system, show that the proposed method considerably improves both computational cost and accuracy for 3-D imaging, where the effective imaging points also increases by decomposing the multiple echoes within same range gate by discriminating the Doppler frequency.

II. SYSTEM MODEL

Figure 1 shows the system model. The model assumes that each target has an arbitrary 3-D shape with a clear boundary and a unique velocity. Antennas are arranged in an array on the $y = 0$ plane to form a multi-static radar configuration. The locations of the transmitting and receiving antennas are defined as $\mathbf{L}_T = (X_T, 0, Z_T)$ and $\mathbf{L}_R = (X_R, 0, Z_R)$, respectively. For each combination of \mathbf{L}_T and \mathbf{L}_R , the recorded electric field is denoted as $s'(\mathbf{L}_T, \mathbf{L}_R, t, \tau)$, where t denotes a fast time and τ denotes a slow time sampled by the pulse repetition interval. $s'(\mathbf{L}_T, \mathbf{L}_R, t, \tau)$ is the output of the Wiener filter of $s(\mathbf{L}_T, \mathbf{L}_R, t, \tau)$ calculated as;

$$s(\mathbf{L}_T, \mathbf{L}_R, t, \tau) = \int_{-\infty}^{\infty} W(\omega) S'(\mathbf{L}_T, \mathbf{L}_R, \omega, \tau) e^{j\omega t} d\omega, \quad (1)$$

where $S'(\mathbf{L}_T, \mathbf{L}_R, \omega, \tau)$ is the form of Fourier transform of $s'(\mathbf{L}_T, \mathbf{L}_R, t, \tau)$ as to t . $W(\omega)$ is defined as

$$W(\omega) = \frac{S_{\text{ref}}(\omega)^*}{(1 - \eta)S_0^2 + \eta|S_{\text{ref}}(\omega)|^2} S_0, \quad (2)$$

where $\eta = 1/(1 + (S/N)^{-1})$, and $S_{\text{ref}}(\omega)$ is the reference signal in the frequency domain, which is the complex conjugate of that of the transmitted signal. S_0 is a constant for dimension consistency. This filter is an optimal MSE (Mean Square Error) linear filter for additive noises. Since we need to deal with multiple reflection signals from multiple objects,

it is quite difficult to determine optimal η , so an appropriate η is determined empirically. $s(\mathbf{L}_T, \mathbf{L}_R, t, \tau)$ is converted to $s(\mathbf{L}_T, \mathbf{L}_R, R, \tau)$, using $R' = ct/2$ with the radio wave speed c . Then, the range-Doppler signals as $S(\mathbf{L}_T, \mathbf{L}_R, R', V'_D)$ is obtained by using the one-dimensional Fourier transform of $s(\mathbf{L}_T, \mathbf{L}_R, R', \tau)$ as to τ . $\mathbf{q} \equiv (\mathbf{L}_T, \mathbf{L}_R, R, V_D)^T$ is defined as the range point (RP), which is extracted from the local maxima of $S(\mathbf{L}_T, \mathbf{L}_R, R', V'_D)$ regarding to R' and V'_D as;

$$\left. \begin{aligned} \frac{\partial |S(\mathbf{L}_T, \mathbf{L}_R, R', V'_D)|}{\partial R'} &= 0 \\ \frac{\partial |S(\mathbf{L}_T, \mathbf{L}_R, R', V'_D)|}{\partial V'_D} &= 0 \\ |S(\mathbf{L}_T, \mathbf{L}_R, R', V'_D)| &\geq \alpha \max |S(\mathbf{L}_T, \mathbf{L}_R, R', V'_D)| \end{aligned} \right\}. \quad (3)$$

This study assumes that each RP is assigned to each scattering center on target boundary, and the conversion from the RPs to target boundary points is regarded as an imaging process.

III. CONVENTIONAL METHODS

Various methods for the reconstruction of target shapes in short-range 3-D imaging have been proposed based on the DAS approach, including beam-forming and Kirchhoff migration. Although the DAS-based methods provide accurate images of point-wise targets, they cannot offer sufficient accuracy for non-point-wise targets; moreover, the computational cost becomes enormous in 3-D imaging due to the signal synthesizing approach with all received signals in each voxel evaluation.

The RPM method has been developed to overcome the above issues [5], and has been extended to the multi-static observation model [9]. This method assumes that a target boundary point exists on an ellipsoid with focal points \mathbf{L}_T and \mathbf{L}_R and major radius R . To extract the target point, this method assumes that the actual target boundary point should be included in all the possible intersection points determined by other range points. To determine a target point $\hat{\mathbf{p}}(\mathbf{q}_i)$ corresponding to range point \mathbf{q}_i , this method extracts the optimal intersection points by assessing the spatial accumulation of intersection points calculated by other range points (called SubRPs) as

$$\hat{\mathbf{p}}(\mathbf{q}_i) = \arg \max_{\mathbf{p}^{\text{int}}(\mathbf{q}_i; \mathbf{q}_j, \mathbf{q}_m) \in \mathcal{P}_i} \sum_{(\mathbf{q}_j, \mathbf{q}_k) \in \mathcal{Q}_{\text{all}}} g(\mathbf{q}_i; \mathbf{q}_j, \mathbf{q}_k) \times \exp \left\{ -\frac{\|\mathbf{p}^{\text{int}}(\mathbf{q}_i; \mathbf{q}_j, \mathbf{q}_k) - \mathbf{p}^{\text{int}}(\mathbf{q}_i; \mathbf{q}_l, \mathbf{q}_m)\|}{2\sigma_r^2} \right\}. \quad (4)$$

Here, $\mathbf{p}^{\text{int}}(\mathbf{q}_i; \mathbf{q}_j, \mathbf{q}_k)$ denotes the intersection points among the three ellipsoids, which is determined by the range points $\mathbf{q}_i, \mathbf{q}_j$, and \mathbf{q}_k , \mathcal{P}_i denotes a set of these intersection points and σ_r is determined considering the spatial density of the accumulated intersection points. \mathcal{Q}_{all} denotes a set of all range points. The weighting function $g(\mathbf{q}_i; \mathbf{q}_j, \mathbf{q}_k)$ is defined as

$$g(\mathbf{q}_i; \mathbf{q}_j, \mathbf{q}_k) = s(\mathbf{q}_j) \exp \left\{ -\frac{D(\mathbf{q}_i, \mathbf{q}_j)}{2\sigma_D^2} \right\} + s(\mathbf{q}_k) \exp \left\{ -\frac{D(\mathbf{q}_i, \mathbf{q}_k)}{2\sigma_D^2} \right\}, \quad (5)$$

where σ_D is determined empirically and $D(\mathbf{q}_i, \mathbf{q}_j)$ denotes the actual separation of the two sets of transmitting and receiving

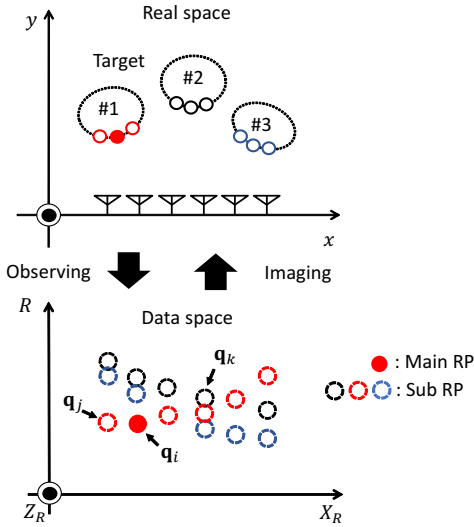


Fig. 2. Range points clustering in RPM scheme.

antennas as

$$D(\mathbf{q}_i, \mathbf{q}_j) = \min \left(\frac{\|L_{T,i} - L_{T,j}\|^2 + \|L_{R,i} - L_{R,j}\|^2}{\|L_{T,i} - L_{R,j}\|^2 + \|L_{R,i} - L_{T,j}\|^2} \right). \quad (6)$$

Note that, in Eq. (4), the optimal combination of \mathbf{q}_l and \mathbf{q}_m is determined by full search for all possible combinations.

Notably, in this method, each range point \mathbf{q}_i is related to a target point $\mathbf{p}(\mathbf{q}_i)$ with one-to-one correspondence. The RPM does not require the connection of range points before processing, allowing the accurate conversion from range points to target points, even in richly interfered cases. The RPM evaluates the degree of accumulation of the intersection points of ellipsoids for a targeted RP as \mathbf{q}_i (named as Main RP) defined by other surrounding range points (named as SubRPs, $\mathbf{q}_j, \mathbf{q}_k$ in Eq. (4)). Figure 2 shows an example conversion between target points and range points in a multi-static configuration; the lower figure shows the cross-sectional view at $(X_T, Z_T, Z_R) = \text{const.}$. In this case, each antenna receives a maximum of three RPs, and RPM converts a MainRP \mathbf{q}_i to target boundary point using surrounding all Sub RPs. However, in the presence of multiple objects, the increasing number of SubRPs seriously increases the computational cost due to the large number of intersection points of the three ellipsoids, which must all be numerically solved. In addition, in the case of multiple objects, the combination of range points from different targets introduces inaccuracy in the calculation of the actual scattering point.

IV. PROPOSED METHOD

Range clustering represents a promising solution for the above issues. In terms of computational efficiency and reconstruction accuracy, the SubRPs are included in the same target cluster of Main RP. In the case of multiple targets, if the Main RP caused from the n -th target, should be processed using only the SubRPs from the n -th target. Figure 2 shows an example of correctly clustered range points. As shown in this figure, only

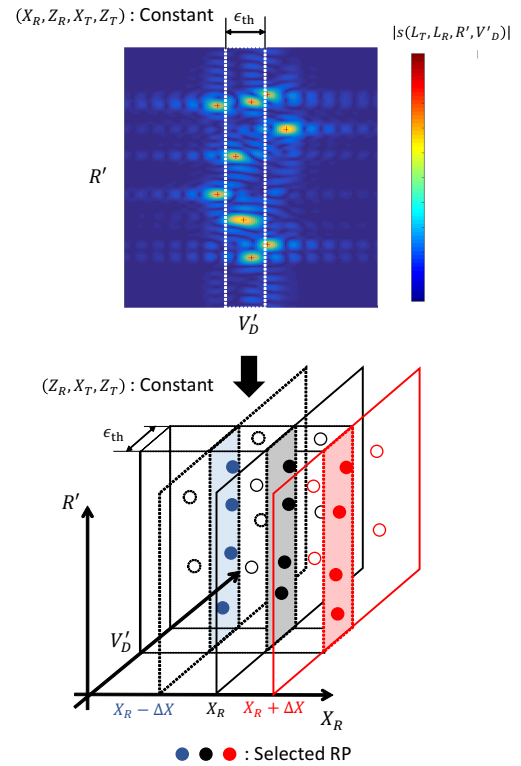


Fig. 3. Example for Doppler based range point clustering.

a set of SubRPs (red broken circles) is necessary to evaluate MainRP (red solid circle), and other RPs may introduce error into the final image. However, it is generally difficult to cluster the range points without *a priori* knowledge of target shape or location, because the range points assuming multiple scatterer are overlapped on data space as Figure 2.

To appropriately cluster SubRPs for each MainRP without *a priori* information about target shape, this paper introduces Doppler-based range points clustering as a preprocessing step within the RPM method. The new method assumes that a group of range points generated from an object has almost the same Doppler velocity, and that each range point can be clustered by its associated Doppler velocity before the RPM process. This method introduces the following criteria for \mathbf{q}_i (denoted as Main RP) and \mathbf{q}_j (denoted as SubRPs);

$$\epsilon(\mathbf{q}_i, \mathbf{q}_j) \equiv |V_{D,i} - V_{D,j}| \quad (7)$$

The set of SubRPs that satisfies $\epsilon(\mathbf{q}_i, \mathbf{q}_j) \leq \epsilon_{th}$ is denoted as \mathcal{Q}_i , and the target point $\hat{\mathbf{p}}(\mathbf{q}_i)$ is calculated in Eq. (4), switching from \mathcal{Q}_{all} to \mathcal{Q}_i . Figure 3 shows the example of Doppler velocity based range points clustering. After extracting range-Doppler map for each antenna combination as L_T and L_R , local maxima of $|S(L_T, L_R, R', V'_D)|$ are extracted as Doppler velocity associated range points. This method confers an additional advantage; multiple range points within the same range gate but with different Doppler velocities can be decomposed, increasing the effective target points.

The procedure of the proposed method is as follows:

- Step 1) Observed data are acquired as outputs of the Wiener filter $s(L_T, L_R, R', \tau)$.
- Step 2) $S(L_T, L_R, R', V'_D)$ are obtained by applying

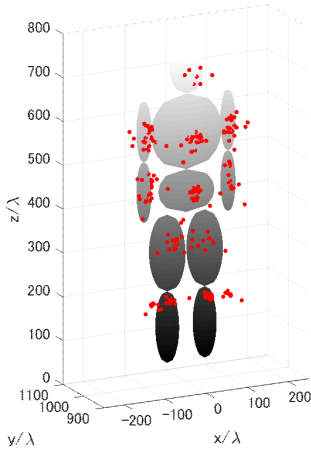


Fig. 4. Scattering center points obtained by the original RPM method in noiseless case.

the one-dimensional discrete Fourier transform to $s(\mathbf{L}_T, \mathbf{L}_R, R', \tau)$ in terms of τ .

Step 3) Range points q_i are extracted from local maxima $|S(\mathbf{L}_T, \mathbf{L}_R, R', V'_D)|$ as to R' and V'_D , and a set of all RPs is defined as \mathcal{Q}_{all} .

Step 4) Range points are clustered by the criteria expressed in Eq. (7) as \mathcal{Q}_i .

Step 5) q_i is converted to a target point $\hat{p}(q_i)$ by RPM using \mathcal{Q}_i in Eq. (4).

Step 6) For each target point $\hat{p}(q_i)$, the associated Doppler velocity $V_{D,i}$ is calculated.

V. EVALUATION IN NUMERICAL SIMULATION

This section evaluates the performance of the original RPM and the newly proposed method using numerical simulation. The transmitting signal forms a pulse modulated signal with a center frequency of 140 GHz and a 10-dB bandwidth of 10 GHz. The center wavelength λ is 2.1 mm, and the theoretical range resolution in the air is 15 mm. The pulse repetition interval is 37.5 μs , and the number of pulse hits is 56. Thus, the Doppler velocity resolution is 0.5 m/s, and the maximum unambiguous range is 20 m. It assumes that the target is a human body approximated as an aggregation of 11 ellipsoids corresponding to the head, upper and lower torsos, arms, and legs (Fig. 1). For simplicity, we consider the stepping motion of human body at same position, where the Doppler velocity of each part is summarized as Table I. The numbers of transmitting and receiving antennas are 4 and 25, respectively, and the minimum array spacing is 50 λ . The received time-series data are generated by GO (Geometrical Optics) approximation without consideration of multiple scattering among targets. The GO is the forward solver based on higher frequency approximation, where the dominant propagation path can be determined by the law of reflection in optics[11]. The motivation for applying GO is that it requires much less computational cost compared with other forward solver, such as FDTD or MoM methods, and we deal with smoothed surface target, the roughness of which is quite larger than the assumed center wavelength (2mm).

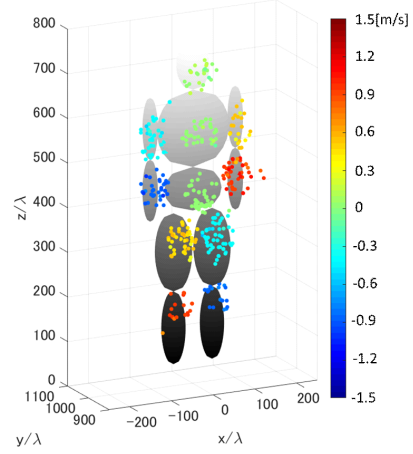


Fig. 5. Scattering center points obtained by the proposed method in noiseless case.

TABLE I

DOPPLER VELOCITIES FOR EACH PART OF HUMAN BODY.

Doppler velocity	Parts
-1.0 m/s	Right lower arm & Left lower leg
-0.5 m/s	Right upper arm & Left upper leg
0 m/s	Head & Lower and Upper torso
0.5 m/s	Left upper arm & Right upper leg
1.0m/s	Left lower arm & Right lower leg

Figures 4 and 5 show the images reconstructed by the original RPM and the proposed methods, respectively. $\epsilon_{\text{th}} = 0.5$ m/s is set in this case. The color of each target point obtained by the proposed method indicates the Doppler velocity. As in Fig. 4, there are some points largely deviated from actual boundary, which are caused by evaluating unnecessary SubRPs in Eq. (4). On the contrary, Fig. 5 demonstrates that the proposed method considerably increases the accurately located scattering centers associated with Doppler velocity, compared with those obtained by the original RPM. This improvement occurred because the range points corresponding to each part of the human body are correctly clustered by difference in Doppler velocity. It should be also noted that the proposed method decomposes multiple range points included in same range resolution based on Doppler velocity; this increases the number of target points, which is another advantage of this method. However, there are non-negligible deviations from an actual boundary for scattering center points reconstructed by both the original and proposed RPM. These errors are mainly caused by the interferences among reflection signals from different parts in the same range gate, then, to reduce these errors, it is promising to introduce a super resolution filter, such as Capon or MUSIC algorithm, which has been demonstrated in [12].

For the quantitative evaluation, the reconstruction error denoted by $e(\mathbf{p}_i^{\text{est}})$ is introduced as

$$e(\mathbf{p}_i^{\text{est}}) = \min_{\mathbf{p}^{\text{true}}} \|\mathbf{p}_i^{\text{est}} - \mathbf{p}^{\text{true}}\|_2, \quad (i = 1, 2, \dots, N_T), \quad (8)$$

where $\mathbf{p}_i^{\text{est}}$ and \mathbf{p}^{true} are the locations of the i -th estimated point and the true target point (namely, the group of discretized points on ellipsoid surface with sufficiently dense sample in

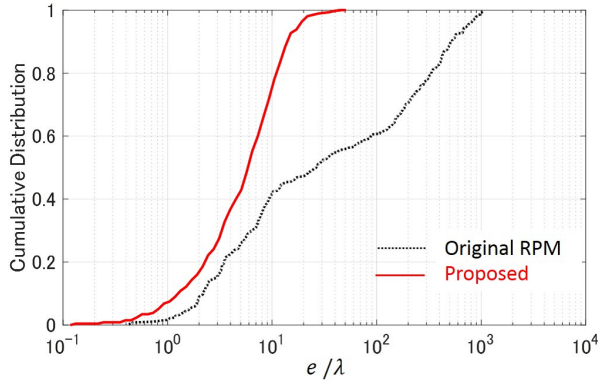


Fig. 6. Cumulative distribution for the reconstruction error e in noiseless case.

this case), respectively, and N_T is the total number of p_i^{est} . Figure 6 shows the cumulative distribution for $e(p_i^{\text{est}})$ in each method. The numbers of reconstructed points satisfying $e < 10\lambda (= 21\text{mm})$ are 116 (41% of total points) for the original RPM method and 441 (74% of total points) for the new method. The calculation times using a Xeon 3.10 GHz processor are 550 s for original RPM and 160 s for the new method.

Performance evaluations in noisy cases are described as follows. To simulate a noisy situation, we added white Gaussian noise to the received time-series data. Table II denotes the average ratio for satisfying $e < 10\lambda (= 21\text{mm})$ and that of mean value of e for the original and new methods in noisy situations at $S/N=30$ dB, where each quantity is averaged over 100 different noise patterns. S/N is defined as the ratio of the peak instantaneous signal power for all polarization data to the average noise power after applying a matched filter. It should be noted that the above definition is the most strict estimation of S/N and considers the locality of signal in both the time and frequency domains, and the signals with $S/N = 30$ dB are practically available by coherent integration procedure, demonstrated in [12]. The results shown in Table II demonstrate that our proposed method still retains more than 70 % points satisfying $e < 10\lambda (= 21\text{mm})$, which is improved from that obtained by the original method as less than 50 %. Finally, it should be noted that, in the actual scenario, we should consider the multiple reflection among objects, which would incur an image distortion in any method. However, this kind of distortion is predicted to be not so serious, because the amplitude of higher order multiple reflections would be considerably lower compared to that of direct scattering, and a time gating process for such kind of multiple reflections also could suppress the false image. It is also our future work to discriminate the multiple reflection components by recognizing Doppler velocities.

VI. CONCLUSION

This paper incorporated a range points clustering algorithm based on Doppler velocity into the RPM method to achieve accurate and high-speed 3-D imaging. The numerical simulation

TABLE II
ACCURACY ANALYSIS AT $S/N=30\text{dB}$.

	Original RPM	Proposed Method
Average ratio satisfying $e < 10\lambda$	49.2 %	72.1%
Average of \bar{e}	12.8λ (26.9mm)	7.8λ (16.4mm)

assuming 140 GHz band UWB radar system and human body imaging issue, has demonstrated that the proposed method remarkably enhances the number of accurately reconstructed points associated with the Doppler velocity by decomposing multiple range points within same range gate, while reducing the required computational time compared to the conventional RPM method. Further acceleration of this method would be done by introducing more efficient algorithm to search the optimal intersection points in Eq. (4), while the present algorithm relies on full search of possible intersection points.

ACKNOWLEDGMENTS

This work is supported by the project "140 GHz band accurate radar system" promoted by Japanese Ministry of Internal Affairs and Communications, Japan.

REFERENCES

- [1] A. J. Devaney, Time Reversal Imaging of Obscured Targets From Multistatic Data, *IEEE Trans. Antennas Propag.*, vol. 53, no. 5, pp. 1600–1610, May, 2005.
- [2] J. M. Lopez-Sanchez, J. Fortuny-Guasch, "3-D radar imaging using range migration techniques," *IEEE Trans. Antennas Propag.*, Vol. 48, No. 5, pp. 728–737, May, 2000.
- [3] F. Soldovieri, A. Brancaccio, G. Prisco, G. Leone, and R. Pieri, "A Kirchhoff-based shape reconstruction algorithm for the multimono-static configuration: The realistic case of buried pipes", *IEEE Trans. Geosci. and Remote Sens.*, vol. 46, no. 10, pp. 3031–3038, Oct., 2008.
- [4] T. Sakamoto, T. Sato, "A Target Shape Estimation Algorithm for Pulse Radar Systems Based on Boundary Scattering Transform," *IEICE Trans. Commun.*, vol. E87-B, no. 5, pp. 1357–1365, July, 2004.
- [5] S. Kidera, T. Sakamoto and T. Sato, "Accurate UWB Radar 3-D Imaging Algorithm for Complex Boundary without Wavefront Connection," *IEEE Trans. Geosci. and Remote Sens.*, vol. 48, no. 4, pp. 1993–2004, Apr., 2010.
- [6] R. Salman, I. Willms "3D UWB Radar Super-Resolution Imaging for complex Objects with discontinuous Wavefronts," *IEEE International Conference on Ultra-Wideband (ICUWB) 2011*, pp. 346–350, Oct., 2011.
- [7] S. Kidera, C. Gao, T. Taniguchi and T. Kirimoto, "Ellipse based image extrapolation method with RPM imaging for through-the-wall UWB radar", *Proc. of 2015 IEEE International Geoscience and Remote Sensing Symposium (IGARSS)*, pp. 385 – 388, July, 2015.
- [8] H. Taki, S. Tanimura, T. Sakamoto, T. Shiina, T. Sato, "Accurate ultrasound imaging based on range point migration method for the depiction of fetal surface," *The Japan Society of Ultrasonics in Medicine 2014*, pp. 51–58, Sep., 2014.
- [9] Y. Sasaki, S. Kidera and T. Kirimoto, "Accurate 3-D Imaging Method Based on Range Points Migration for 140GHz-band Radar," *IEEE International Conference on Ubiquitous Wireless Broadband (ICUWB) 2015*, Montreal, Canada, Oct., 2015.
- [10] Y. Kim and H. Ling, "Human Activity Classification Based on Micro-Doppler Signatures Using a Support Vector Machine ", *IEEE Trans. Geosci. and Remote Sens.*, vol. 47, no. 5, pp. 1328–1337, May, 2009.
- [11] V. U. Zavorotny and A. G. Voronovich, Comparison of geometric optics and diffraction effects in radar scattering from steep and breaking waves", *IEEE International Geoscience and Remote Sensing Symposium, IGARSS 2007.*, July, 2007.
- [12] S. Kidera, T. Sakamoto and T. Sato, "Super-Resolution UWB Radar Imaging Algorithm Based on Extended Capon with Reference Signal Optimization," *IEEE Trans. Antennas. & Propagation.*, vol.59, no. 5, pp. 1606–1615, May, 2011.